



Factors Controlling Reservoir Quality of a Paleozoic Tight Sandstone, Rub' al Khali Basin, Saudi Arabia

Abdullah Alqubalee¹ · Lameed Babalola¹ · Osman Abdullatif² · Mohammed Makkawi²

Received: 11 December 2018 / Accepted: 25 April 2019 / Published online: 8 May 2019
© King Fahd University of Petroleum & Minerals 2019

Abstract

The heterogeneity of depositional and diagenetic controls on the reservoir quality of tight sandstones is a major challenge. Understanding which factors are the most influential is significant for improving reservoir evaluation and prediction. This study utilized sedimentological core descriptions, thin-section petrography, quantitative evaluation of mineralogy by scanning electron microscope, X-ray diffractometry, scanning electron microscopy and porosity–permeability measurements to define and characterize the factors that control reservoir quality in the Upper Ordovician Sarah Formation of the Rub' al Khali Basin. Four facies associations (FA), including fluvial (FA1), glaciolacustrine delta (FA2), subglacial (FA3) and glaciofluvial (FA4), have been recognized. The results show that the highest reservoir quality was enhanced by feldspar dissolution in FA1. The development of its reservoir quality was, however, partially limited by compaction, and authigenic pore filling and grain coating with the clay mineral, illite. The lowest reservoir quality, related to FA3, appears to have been influenced by the detrital matrix content, compressibility and siderite cement precipitation. The presence of a detrital matrix, anhydrite and barite cement, and grain compaction reduced the reservoir quality in FA2. On the other hand, intergranular porosity, and fractures that facilitated the development of dual porosity and permeability systems in this FA, might have slightly enhanced its reservoir quality. Factors such as grain-size distribution and sorting influenced the reservoir quality of all the FAs, but these were the main controls on the reservoir quality of FA4, in addition to compaction. The reservoir quality of this FA might have also been improved by fractures and the dissolution of unstable grains.

Keywords Glaciogenic deposits · Reservoir quality controls · Sandstone diagenesis · Unconventional tight sandstone · Heterogeneity

1 Introduction

Tight gas sandstone is one of the unconventional natural gas resources that are huge in quantity, but costly to exploit. Advanced hydraulic fracturing technologies are required to make them productive [1]. The definition of a tight gas sandstone varies according to the economic perspectives of different countries [2–4]. Tight gas sandstones and shales

occurring in Paleozoic siliciclastic sequences are major unconventional resources in Saudi Arabia [5, 6]. They represent significant portions of the proven natural gas reserves (about 297.6 trillion cubic feet [7]) in the country. The Upper Ordovician Sarah Formation is considered to be a potential tight gas reservoir in the Rub' al Khali Basin, and it is a proven tight gas reservoir elsewhere in Saudi Arabia. The formation is stratigraphically overlaying the Qasim Formation and overlaid by the Silurian source rock—the Qusaiba Formation (Table 1).

Porosity and permeability are the major indicators of reservoir quality, which is, in turn, one of the key controls on the exploration and evaluation of hydrocarbon reservoirs [8, 9]. In siliciclastic reservoirs, these two petrophysical properties are affected by several factors, including sediment depositional properties and post-depositional processes (diagenesis). The depositional properties include lithological type, mineralogical composition, and texture (grain size,

✉ Abdullah Alqubalee
qubalee@live.com

✉ Lameed Babalola
lbabalola@kfupm.edu.sa

¹ Center for Integrative Petroleum Research, College of Petroleum Engineering and Geosciences, King Fahd University of Petroleum and Minerals, Dhahran, Saudi Arabia

² Geosciences Department, College of Petroleum Engineering and Geosciences, King Fahd University of Petroleum and Minerals, Dhahran, Saudi Arabia



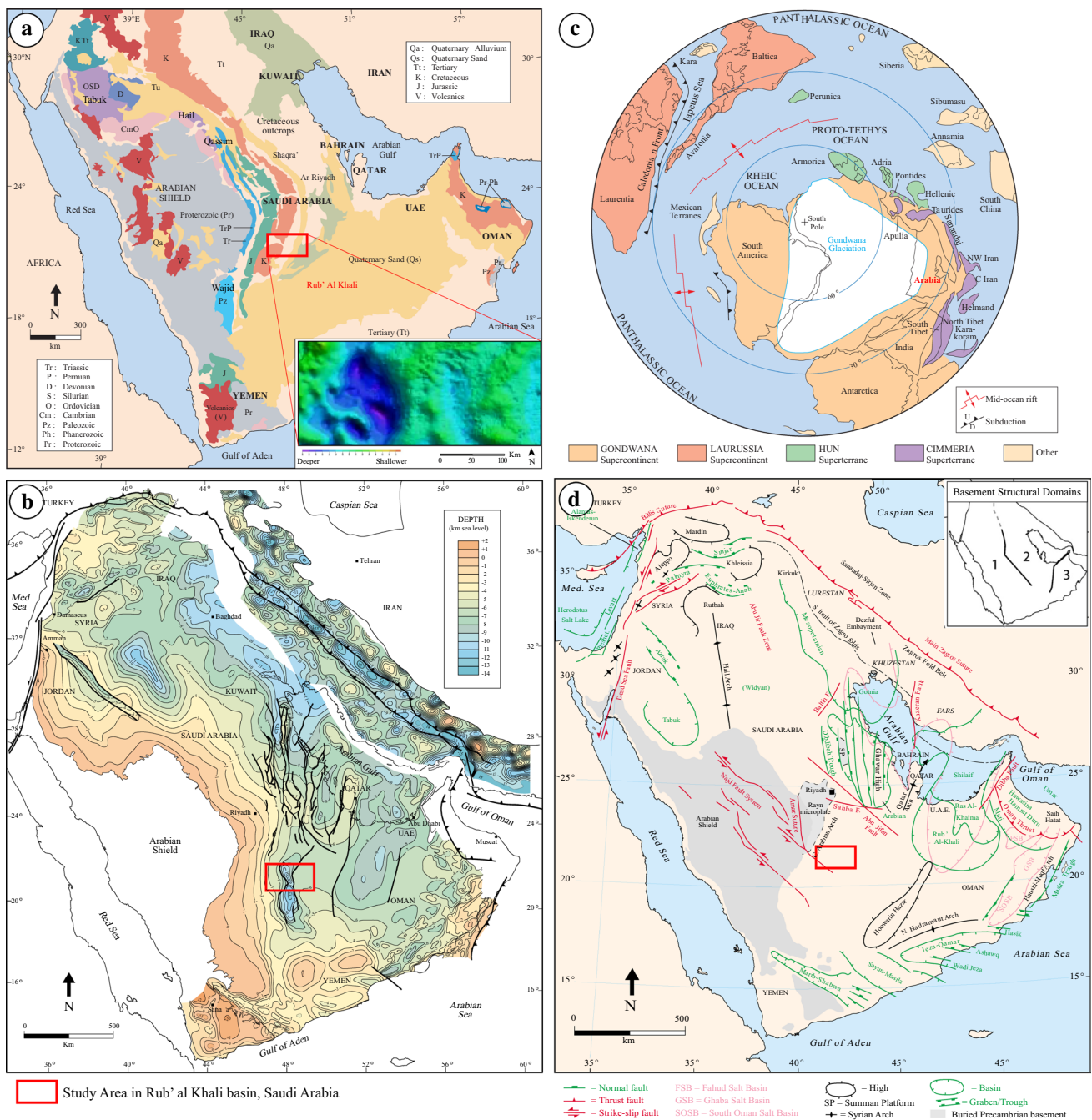


Fig. 1 **a** Surface geological map of the Arabian Peninsula, modified after Al-Husseini [42]. Inset map shows basement depressions (in blue) on the gravity map of the Saudi Geological Survey. **b** Basement depth map of the Arabian Peninsula, modified after Konert et al. [11]. **c** Paleogeographic reconstruction of the Late Ordovician to Early Silurian, modified after Ruban et al. [43]. **d** Tectonic and structural elements of the Arabian Peninsula, modified after Ziegler [44]. Inset map shows general structural domains of the basement, after Stern and Johnson [14]

Cambrian–Ordovician sandstones [31]. Exploration activities on the Upper Ordovician deposits in the Rub’ al Khali Basin have revealed that the facies is heterogeneous [32, 33] and the reservoir rocks of the formation, which is sealed by Qusaiba shales and tight diamictites, have been controlled by multiple factors, such as burial depth, facies and paleogeographic setting [33].

modified after Ruban et al. [43]. **d** Tectonic and structural elements of the Arabian Peninsula, modified after Ziegler [44]. Inset map shows general structural domains of the basement, after Stern and Johnson [14]

3 Samples and Methods

The facies of core samples retrieved from six exploratory wells that penetrated the Sarah Formation in the Rub’ al Khali Basin have been described, grouped and interpreted by Alqubalee et al. [10]. Herein, the core descriptions and interpretations are integrated with further petrographic studies,

Table 2 Facies codes, descriptions and interpretations of four recognized paleoenvironmental FAs, after Alqubalee et al., [10]

Wells	Facies Association	Facies codes	Description	Other remarks	Interpretation
B	FA3	Dcm	Clast-supported, massive diamictite	Polymictic	Debris flow
D		Dmm	Matrix-supported, massive diamictite	Fractures	
F				Higher matrix contents	
F		Dms	Matrix-supported, stratified diamictite	Intercalated with fissile shale	
B		Ds	Sandy massive diamictite, slightly graded	Share deformation structures, gradings	
E	FA4	GRfu	Upward fining granules	Gradings, erosional scours	Rapid deposition by highly concentrated, non-cohesive sediment-gravity flows
		GRh	Horizontally bedded granules		
A	FA1	Sm	Massive sandstone, or faint lamination	Faint parallel lamination	Rapidly deposited by sediment-gravity flow
B	FA2			Gray to dark gray, mud patches, stylolites.	
C				Gray to dark gray, mottles, erosional scours, stylolites	
D	FA4			Argillaceous, erosional scour	
E				Occasionally graded, erosional scours	
A	FA1	Sd	Deformed sandstone	Dish structures, fractures	Water escape deformation formed by liquidization
B	FA2			Folded lamina, veins, boudins, fractures, share planes	Deformation due to direct glacial movements
E	FA4			Thrust planes, share planes, stratification	Glacial deformation?
		St	Trough cross-stratified sandstone	Medium-grained	3D dunes deposited from turbulent, high-energy currents
A	FA1	Sr	Sandstone with ripples	Occasionally disrupted	Lower flow regime
C	FA2			Fine-grained, occurring within thin beds	
B	FA3	Fm	Massive siltstone, claystone/shale	Silty	Deposited by suspension
F				Fissile, intercalated with Dms and Dmm	

X-ray diffractometer (XRD), scanning electron microscope (SEM), quantitative evaluation of mineralogy by scanning electron microscopy (QEMSCAN), and petrophysical (porosity and permeability) analyses.

Using a petrographic microscope, 140 thin sections were analyzed for identifying the microdepositional and microdiagenetic facies. Records of the grain size and sorting, which were visually estimated from the thin sections, were taken after analyzing the bulk mineralogical composition of 50 pulverized samples, selected based on facies changes, using a *Rigaku Ultima IV* XRD.

To better quantify the mineralogical compositions of the samples, 24 thin sections were analyzed using the QEMSCAN, which was preceded by carbon coating using a Q150T Quorum EMS 150R ES. An operating X-ray beam voltage of 15 kV, with a beam current of 10 nA (± 0.05), was applied. The measurements were collected in field image scan mode

on an area of 1 cm², with 5- μ m-point spacing. The measurements took about 7.5 h per sample. Several commonly used preprocessors and filters, such as field stitch, granulator, boundary phase processor, were applied during the data processing phase. As a result, an areal percentage could be calculated for each mineral in each sample.

The clay mineral types and morphologies in 24 samples, representing the recognized facies associations (FAs), were investigated in a SEM coupled to a JEOL JSM-6610LV energy-dispersive X-ray (EDX).

Porosity and permeability measurements were obtained from 140 plugs from the cores, drilled at approximately 1-ft intervals, using a helium porosimeter and an automated permeameter-porosimeter (AP-608). The latter technique uses Boyle's law to measure pore volumes, while Klinkenberg-corrected permeability measurements were calculated based on the pressure decay concept. Both porosity

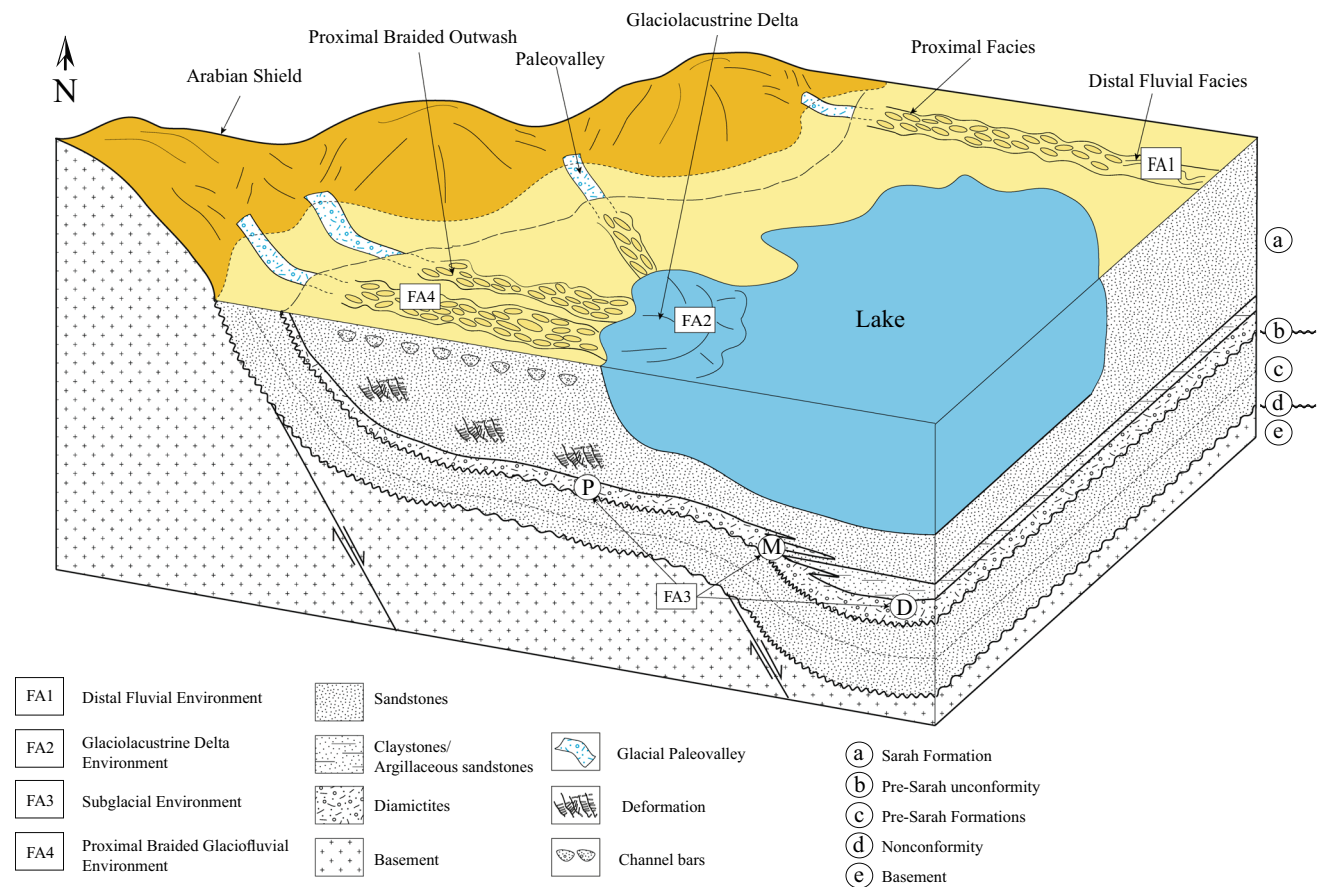


Fig. 2 Conceptual depositional model of the Sarah Formation in the studied and surrounding areas, after Alqubalee et al. [10]

and permeability measurements were also acquired from all the plugs at 500 psi. In addition, 26 selected intact plugs were remeasured for both porosity and permeability at higher confining pressures (1000 psi, 2000 psi, 4000 psi and 5000 psi), where porosity/permeability outliers occurred in porosity–permeability crossplots; 15 plugs were remeasured at 500 psi for quality assurance and quality control.

4 Results

4.1 Depositional Facies

4.1.1 Facies Associations

Four FAs, representing six core samples recovered from the Sarah Formation in the Rub’ al Khali Basin, have been identified and reported by Alqubalee et al. [10]. These FAs included massive- to ripple-marked sandstones (FA1), grayish massive sandstones (FA2), diamictites (FA3) and graded to massive, partially deformed sandstones (FA4). Because of the lithofacies identifications form the basic reference point for this study, a summary of the facies and depositional settings of the studied cores from Alqubalee et al. [10] is given below

(Fig. 2), and the facies codes mentioned here are explained in Table 2.

- FA1, representing a 28.90-ft (8.81-m)-thick core interval, occurs only in Well A (Fig. 3f) and comprises predominantly fine- to medium-grained, moderately to poorly sorted sandstones (Fig. 4a). It encompasses massive (Sm; Fig. 5a), ripples-marked (Sr; Fig. 5b) and water-escape-deformed (Sd) sandstone facies. The sediments of FA1 have been interpreted as fluvial deposits.
- FA2, with a total thickness of 58.30 ft (17.77 m), occurs in Wells B (Fig. 3e) and C (Fig. 3c). It consists of grayish massive sandstone (Sm; Fig. 5c), deformed argillaceous sandstone (Sd; Fig. 5d) and claystone (Fm) in Well B, and mottled to massive sandstones (Sm; Fig. 5e), associated with erosional scours, stylolites and occasional thin layers of ripple-marked sandstone, in Well C. This FA, which is predominantly poorly sorted (Fig. 4b), clay to medium-grained, occasionally coarse-grained, sandstone, has been interpreted as the product of a glaciolacustrine delta setting.
- FA3 occurs in Wells B (Fig. 3e), D (Fig. 3d) and F (Fig. 3b), and has a thickness of 7.61 ft (2.32 m), 13.12 ft (4 m) and 7.28 ft (2.22 m), respectively. This FA is composed

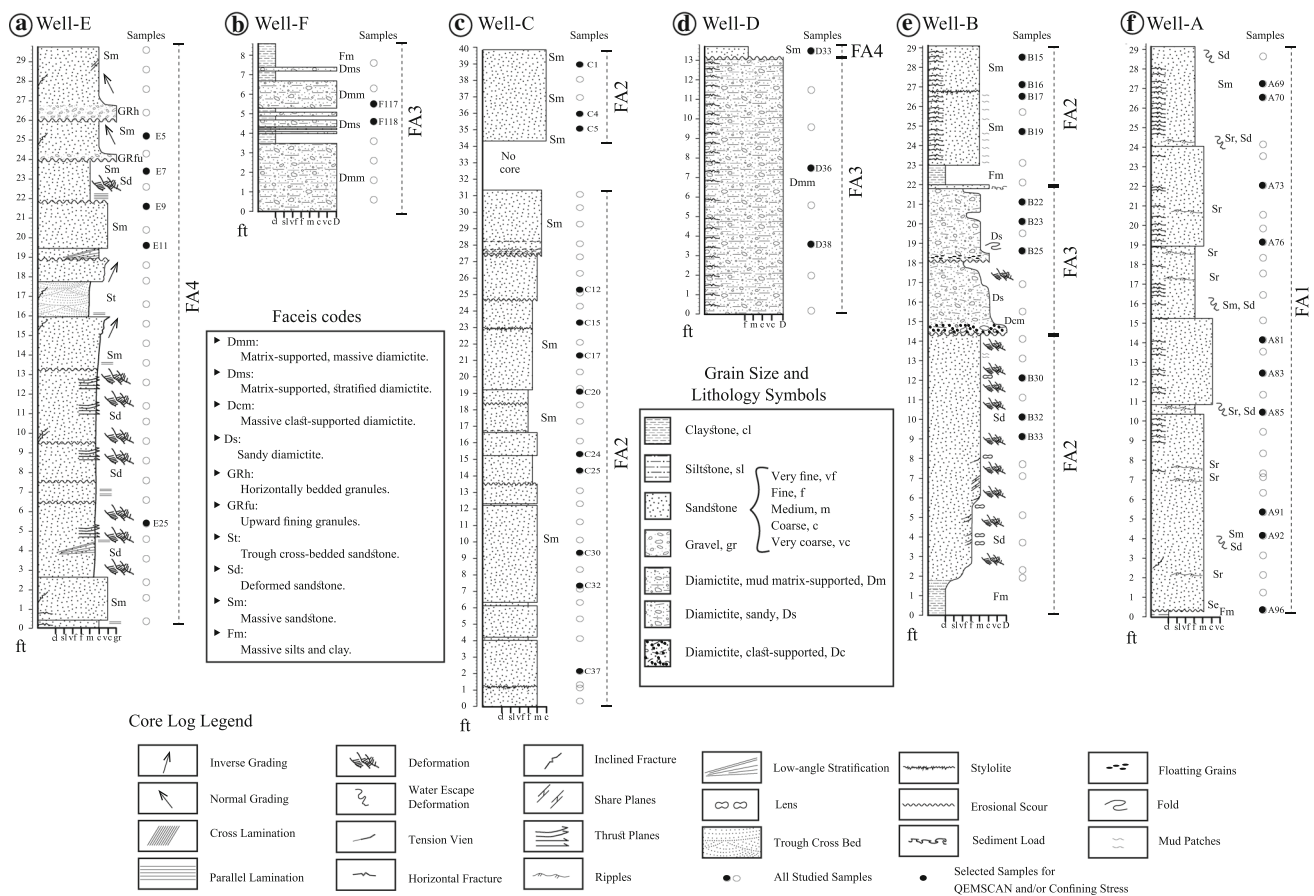


Fig. 3 Sedimentological logs for all the studied wells. FA1: fluvial, FA2: glaciolacustrine delta, FA3: subglacial and FA4: glaciofluvial outwash facies, modified after Alqubalee et al. [10]

of massive matrix-supported (Dmm; Fig. 5i), massive clast-supported (Dcm; Fig. 5h), stratified matrix supported (Dms; Fig. 5j) and sandy (Ds; Fig. 5f-g) diamictites. These facies have been interpreted as subglacial deposits.

- FA4, which is 29.69 ft (9.05 m) thick in Well E (Fig. 3a) and 0.49 ft (0.15 m) thick in Well D (Fig. 3d) is characterized by a range of facies, including massive (Sm), deformed (Sd; Fig. 5k), trough cross-stratified (St) sandstones, which are overlain by two fining-upward cycles, a graded to massive, medium- to coarse-grained and granular-grained sandstone (GRfu; Fig. 5l), and a graded to massive, stratified granular-grained sandstone (GRh). FA4 is generally composed of medium- to coarse-grained and poorly to very poorly sorted sediments (Fig. 4d), which are occasionally associated with erosional scours. FA4 has been interpreted as glaciofluvial outwash deposits.

4.2 Mineralogy and Texture

Quartz (monocrystalline and polycrystalline), feldspars (orthoclase, microcline and albite), micas (muscovite and biotite) and illite, occurring in varying amounts, are the main detrital mineralogical components recognized in all FAs.

Trace heavy minerals, such as rutile, zircon and apatite, and varying amounts of authigenic clay minerals (illite, smectite, kaolinite and glauconite), evaporites (anhydrite, siderite and barite), carbonates (calcite and dolomite) and pyrite were also identified in the investigated samples. The authigenic minerals range from 0 to 30%, and vary from one sample to another.

The fluvial facies of Well A (Sm, Sr and Sd; FA1) are very fine- to medium-grained, angular to rounded, loose to compacted and moderately sorted subarkose sandstones ($Q_{91}F_7L_1$; Fig. 6b). The grain contacts are mainly point to long, but also show concavo-convex and sutured contacts in several samples. The monocrystalline quartz, ranging from ~85 to ~92.3% (Fig. 7a), is the most dominant mineral in this FA. The QEMSCAN analysis showed that the amount of K-feldspar, which is highly affected by diagenetic dissolution, is less than 2% in the facies (Table 3). Authigenic clay minerals mainly occur as pore fillings and occasionally as grains coated with illite; they account for ~2 to ~8% of the bulk mineralogical composition.

The glaciolacustrine delta facies (Sm, Sd and Fm; FA2) in Wells B and C are mainly composed of quartz arenite ($Q_{96}F_3L_1$) and sublithic arenite ($Q_{91}F_3L_6$; Fig. 6c). Their

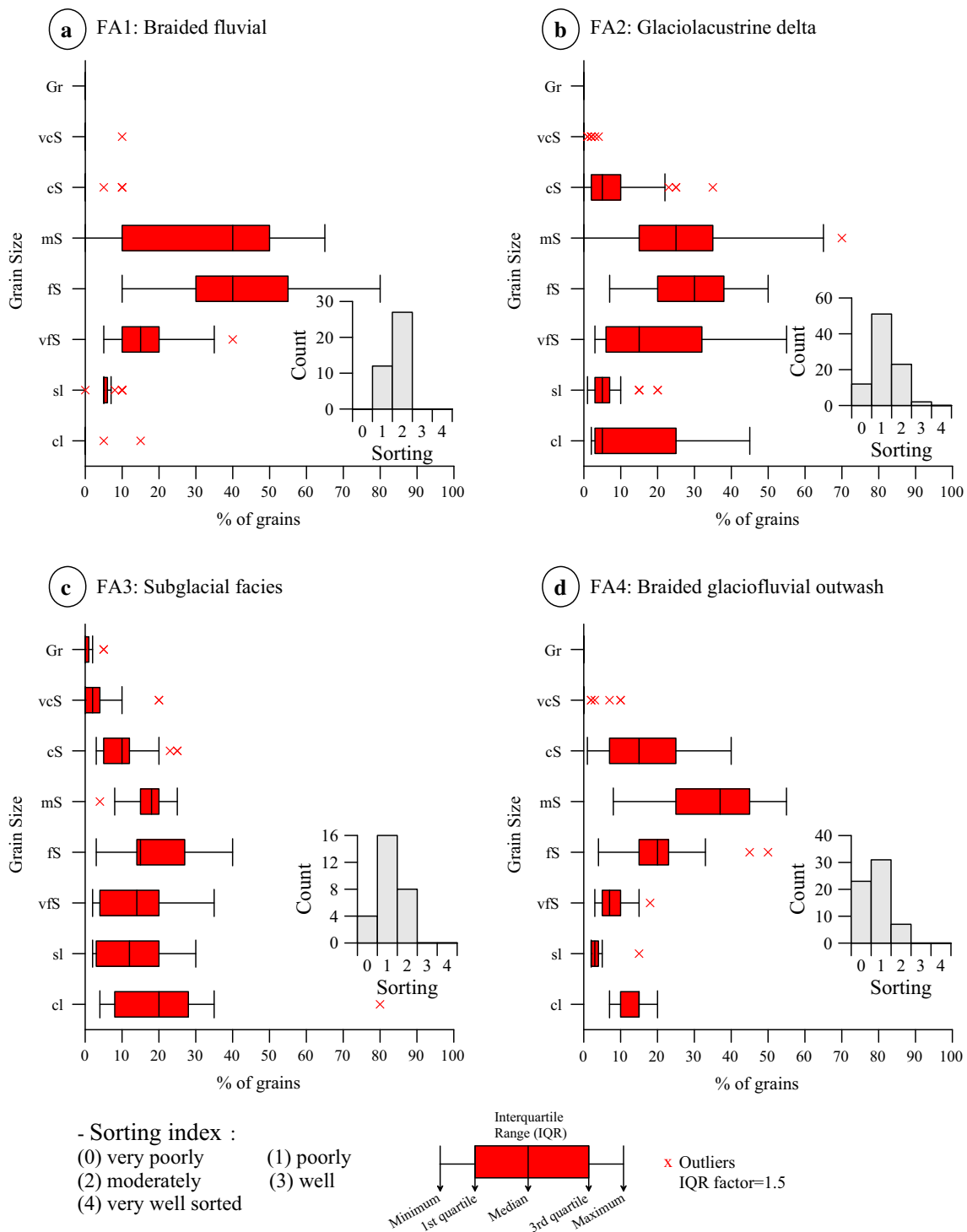


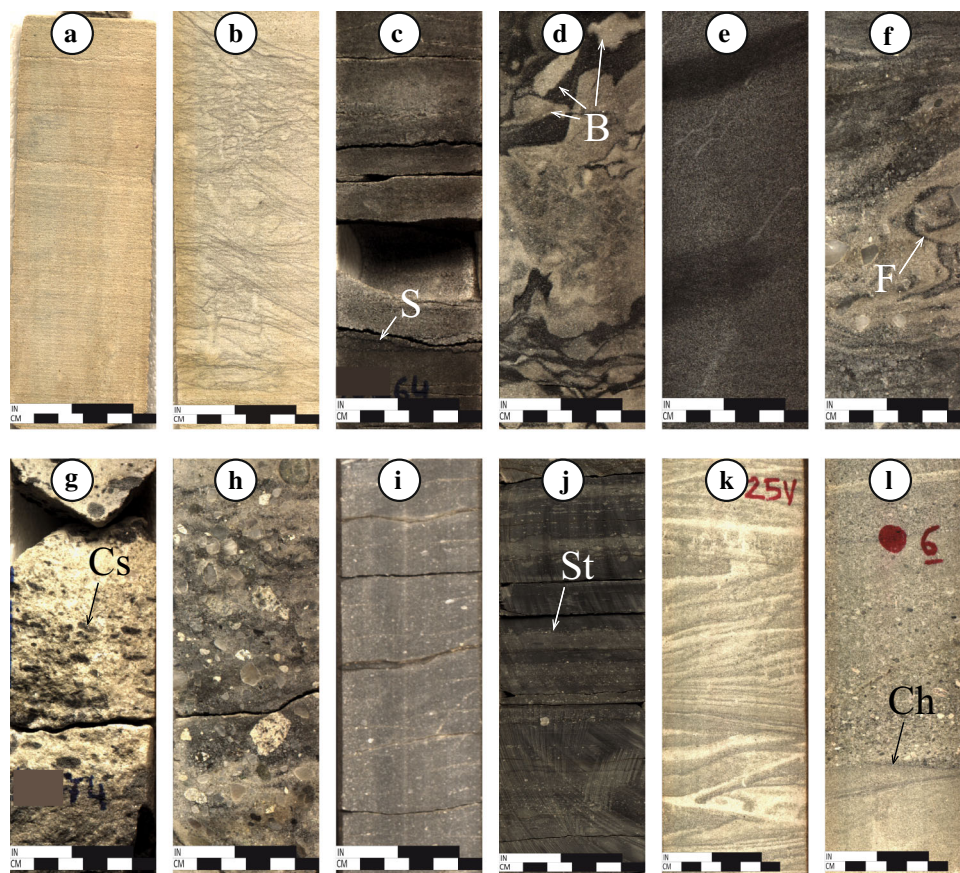
Fig. 4 Box-and-whisker plots of grain size, and histograms of sorting, for all FAs. **a** FA1 is dominantly characterized by fine- (fS) to medium-grained (mS), moderately sorted sandstones. **b** FA2 and **c** FA3 show

significant variability in their grain sizes, while the grain sorting in both is predominantly poor. **d** FA4 is dominated by medium- (mS) and coarse-grained (cS), poorly and very poorly sorted sandstones

grains are predominantly poorly sorted, occasionally moderately sorted, angular to rounded, and very fine to very coarse, with a matrix content (clay and silt) varying from

0 to 40% (Fig. 7b–d). FA2 shows variable grain contacts and significant mineralogical variations, which is most likely due to diagenetic cementation. The detrital quartz (mainly

Fig. 5 Representative core photographs of all FAs. FA1 includes, **a** massive sandstone (Sm) and **b** rippled sandstones (Sr) in Well A. FA2 contains, **c** grayish massive sandstone (Sm) with stylolite (S) and **d** deformed argillaceous sandstone (Sd) with boudins (B) in Well B, and **e** another grayish massive sandstone (Sm) in Well C. FA3 includes, **f** sandy diamictite (Ds) with a folded lamina (F), **g** oriented floating clasts (Cs) within the Ds facies, **h** clast-supported diamictites (Dcm), **i** a massive matrix-supported diamictite (Dmm), and **j** stratified (St)-matrix-supported diamictite (Dms). FA4 includes **k** deformed sandstone and **l** channel base contact (Ch) between massive and graded sandstone



monocrystalline) ranges from 75.6 to ~94%, infrequently decreased where evaporitic minerals (anhydrite 0%–21%, siderite 0%–~3% and barite 0%–2.4%) become increased in the Sm facies, or by increased detrital illite (0.3%–~7.5%) and micas (muscovite 0.5%–~10% and biotite <1%; Fig. 7f) in the Sd facies. Also, K-feldspar and albite (Fig. 7e) occur in minor amounts, ranging from <0.1 to 4.68% in FA2, particularly in Well C.

The subglacial facies (FA3), including Dmm, Dms, Dcm and Ds, is mainly represented by sublithic arenite (Q₉₂F₁L₆), with a few samples being quartz arenite (Fig. 6d). The grain size ranges from the clay to pebble fractions, which are poorly sorted, with angular to rounded grains, and ~40% matrix content only in the Dmm facies (Fig. 7h–j). Most of the grains are loose in the matrix, which displays floating grain texture, but there are also point and long contacts between some of the grains, especially in the Ds facies (Fig. 7g). The quartz content, mainly monocrystalline with minor amounts of polycrystalline (Fig. 7g, j), is higher in the Ds and Dcm facies of Well B (ranging from ~72 to ~81%) than in the Dmm and Dms facies (~54.5 to ~66%) in Wells D and F, where other detrital minerals, such as illite (15–~22%), K-feldspar (~5–7%), albite (0.5 to ~5%) and biotite (~5–13%; Fig. 7i), are appreciably present. Siderite cement in the Ds facies (FA3) ranges from 0 to ~19.5%. Pyrite occurred in

variable amounts (0.1–2.3%) in almost all the diamictites facies (Fig. 8i).

The sublithic arenite (Q₉₂F₁L₇; Fig. 6e) of the glaciofluvial facies (FA4) is characterized by moderately to poorly sorted (Fig. 7k–l), angular to rounded, fine to very coarse grains. Point and long grain contacts are dominant and are commonly associated with concavo-convex and sutured contacts. Based on the QEMSCAN data, FA4 is also dominated by quartz (~59.5–90.21%; Table 3), with minor amounts of K-feldspar (<3.25%; Fig. 7k), albite (<1.18%), muscovite (<1%) and biotite (~1–3.63%). Diagenetic minerals, including siderite (29.68%, occurred in the Sm facies of Well D), authigenic illite (~1–5.12%), chlorite (<0.25%) and dolomite (≤1%), are also present in this FA.

4.2.1 Diagenetic Processes

In addition to lithification of the sediments after deposition and fracture development, the main results of diagenetic processes observed in all the identified FAs in this study include compaction, dissolution and cementation. Diagenetic recrystallization, alteration and replacement of minerals also occurred rarely. Each FA showed various degrees of diagenesis, ranging from slight, as in the subglacial facies (FA3), to severe, as in the fluvial facies (FA1).

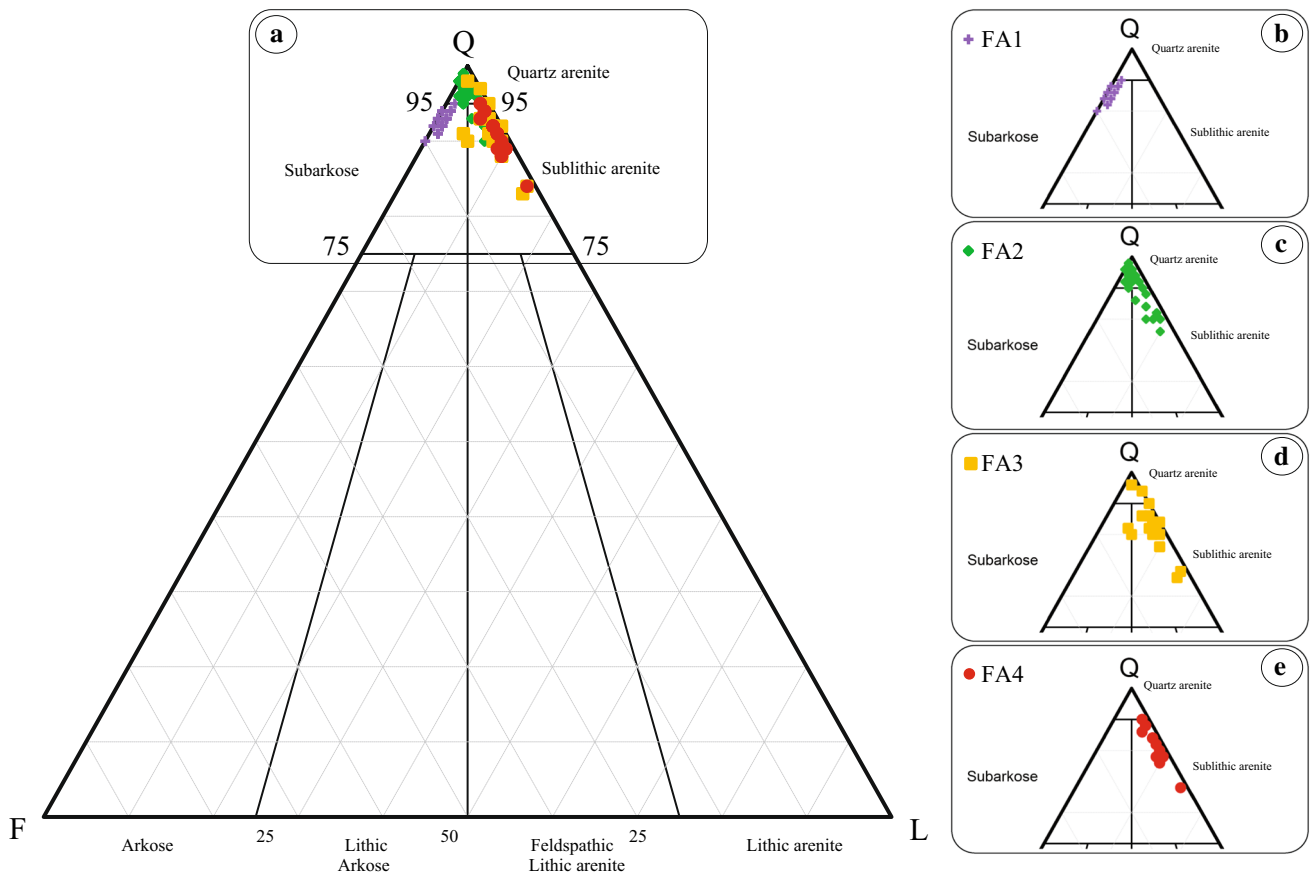


Fig. 6 Petrographic sandstone classification of **a** all FAs, ranging from **b** subarkose in the fluvial facies (FA1) to quartz arenite and sublithic arenite in the glaciolacustrine delta facies (FA2), to mainly sublithic arenite in both the subglacial (FA3) and glaciofluvial outwash (FA4) facies, after Alqubalee et al. [10]

4.2.2 Dissolution and Compaction

Relative to the other FAs, the fluvial facies (Well A), in which almost all the feldspar grains were either partially or completely dissolved, has been highly affected by grain dissolution. The feldspar grain dissolution appears to have followed the grain cleavages, as clearly observed in plane-polarized optical microscopy (Fig. 8b) and the SEM (Fig. 8c). Virtually complete feldspar dissolution was recognized by the remnants of grains that were barely preserved in the fluvial facies (FA1, Well A). Although partially dissolved feldspars were observed in the glaciofluvial facies (FA4, Well E) and glaciolacustrine delta (FA2, wells B and C) facies, unaltered feldspar grains are also commonly preserved in these FAs (e.g., Figure 7k) and in the subglacial facies (FA3).

Mechanical grain compaction was observed in the fluvial (FA1), glaciofluvial (FA4) and part of the glaciolacustrine delta (FA2, Sm; Fig. 8d) facies. This showed microscale heterogeneity where compaction bands associated with cementation and/or porosity (Fig. 8e, h) were present. Chemical grain compaction, resulting from pressure dissolution of grain contacts, was indicated by suture grain contacts and/or

stylolites (Fig. 8d), mainly in the Sm facies of the fluvial (FA4) and glaciolacustrine delta (FA2) facies, where individual quartz grains were distorted (Fig. 8e). Fractures caused by glacial deformation were developed in intervals rich in matrix content, such as in the Sd (FA2, Fig. 7c) and Dmm (FA3, Fig. 7h) facies.

4.2.3 Cementation

Cementation is one of the significant diagenetic processes that also showed microscale heterogeneity in all the studied FAs. The cement content in the facies varied from 1 to 30%. Authigenic illite represented the main cementation agent, being present in the fluvial (FA1, Fig. 8a, c) and glaciofluvial outwash (FA4) facies. It was occasionally associated with trace siderite and iron oxides (Fig. 8b). The Sm facies of Well D (FA4) was highly cemented by siderite (Fig. 8k), and syntaxial quartz overgrowth was present in the fluvial (FA1) and glaciofluvial (FA4) facies. Quartz overgrowth was occasionally well developed in the glaciofluvial FA (Fig. 8l).

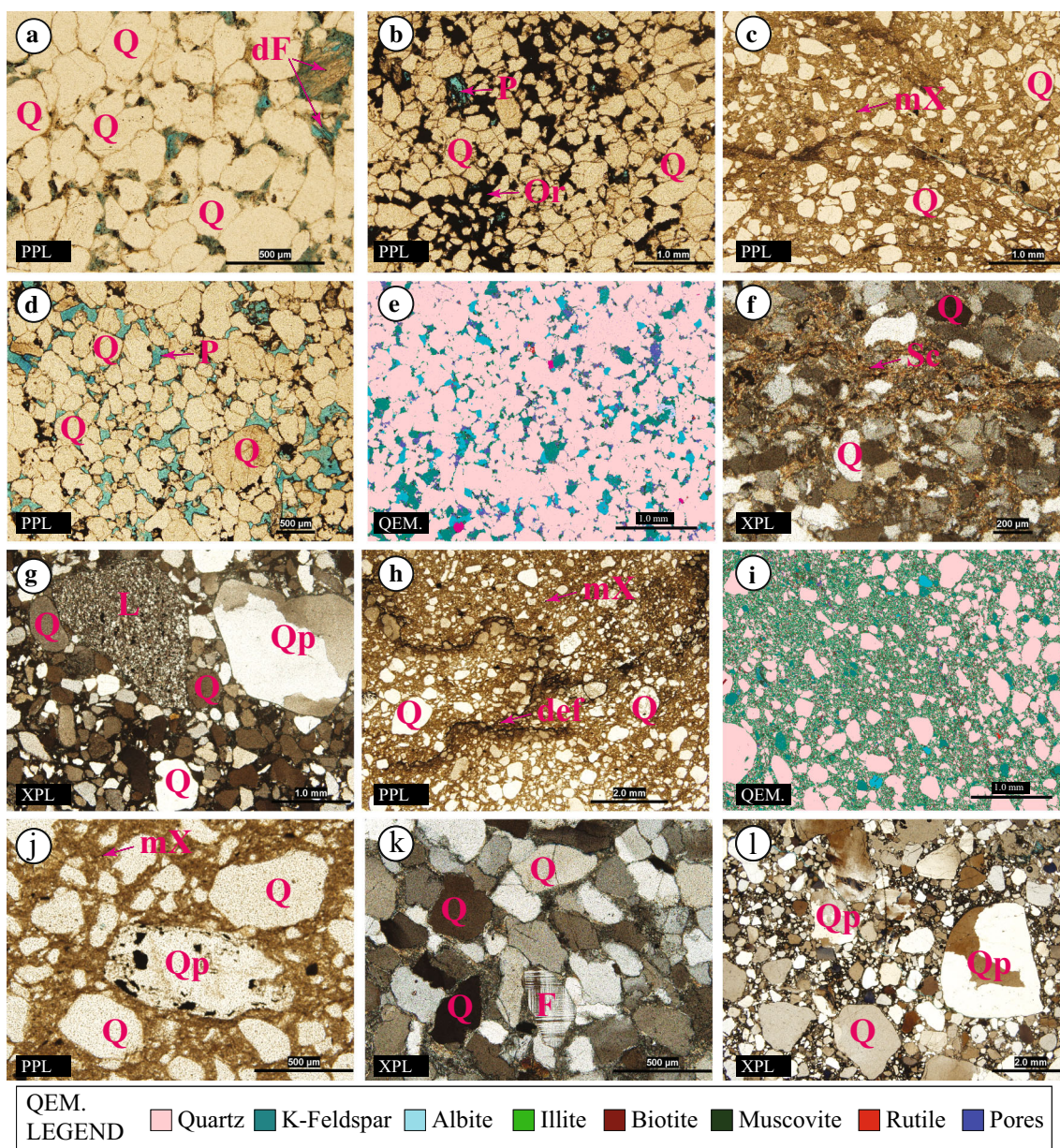


Fig. 7 Representative microdepositional facies of all FAs. **a** Monocrystalline quartz (Q) associated with dissolved feldspar (dF) in the Sm facies of Well A (FA1) in plane-polarized light (PPL). **b** Primary porosity (P) occupied by organic matter (Or) in the Sm facies of Well B (FA2). **c** Pore-filling matrix (mX) in the Sd facies of Well B (FA2). **d** Primary porosity (P) in the Sm facies of Well C (FA2). **e** QEMSCAN image (QEM) of quartz, K-feldspar and albite in the Sm facies of Well C (FA2). **f** Sericite (Sc) filling the pores in Well C (FA2). **g** Monocrystalline (Q) and polycrystalline (Qp) quartzes and lithic rock fragment (L)

in the Ds facies of Well B (FA3). **h** Deformation (def) in the Dmm facies of Well D (FA3). **i** Detrital illite and micas in the Dmm facies of Well F (FA3). **j** Matrix-surrounded mono- and polycrystalline quartz grains in the Dmm facies of Well D (FA3). **k** A well-preserved K-feldspar (microcline) grain in predominantly compacted quartz grains in the Sm facies of Well E (FA4). **l** Poorly sorted mono- and polycrystalline quartz grains in the GRh facies of Well E (FA4)

The glaciolacustrine delta facies (FA2) was characterized by the presence of anhydrite (Fig. 8f), barite (Fig. 8g) and occasional siderite cement. The evaporite cementation occurred in variable amounts in FA2, where it ranged from >0.1 to 21.39%. For instance, in the Sm facies of the upper and lower parts of Well C (FA2), anhydrite and barite

cements, respectively, did not completely occlude the primary pores in several parts of the samples; a certain amount of porosity was also preserved and was occasionally filled with organic matter (Fig. 8e). Only in the subglacial Ds facies (Well B, FA3), grains were cemented by siderite, associated with isolated matrix-supported partings (Fig. 8j), while

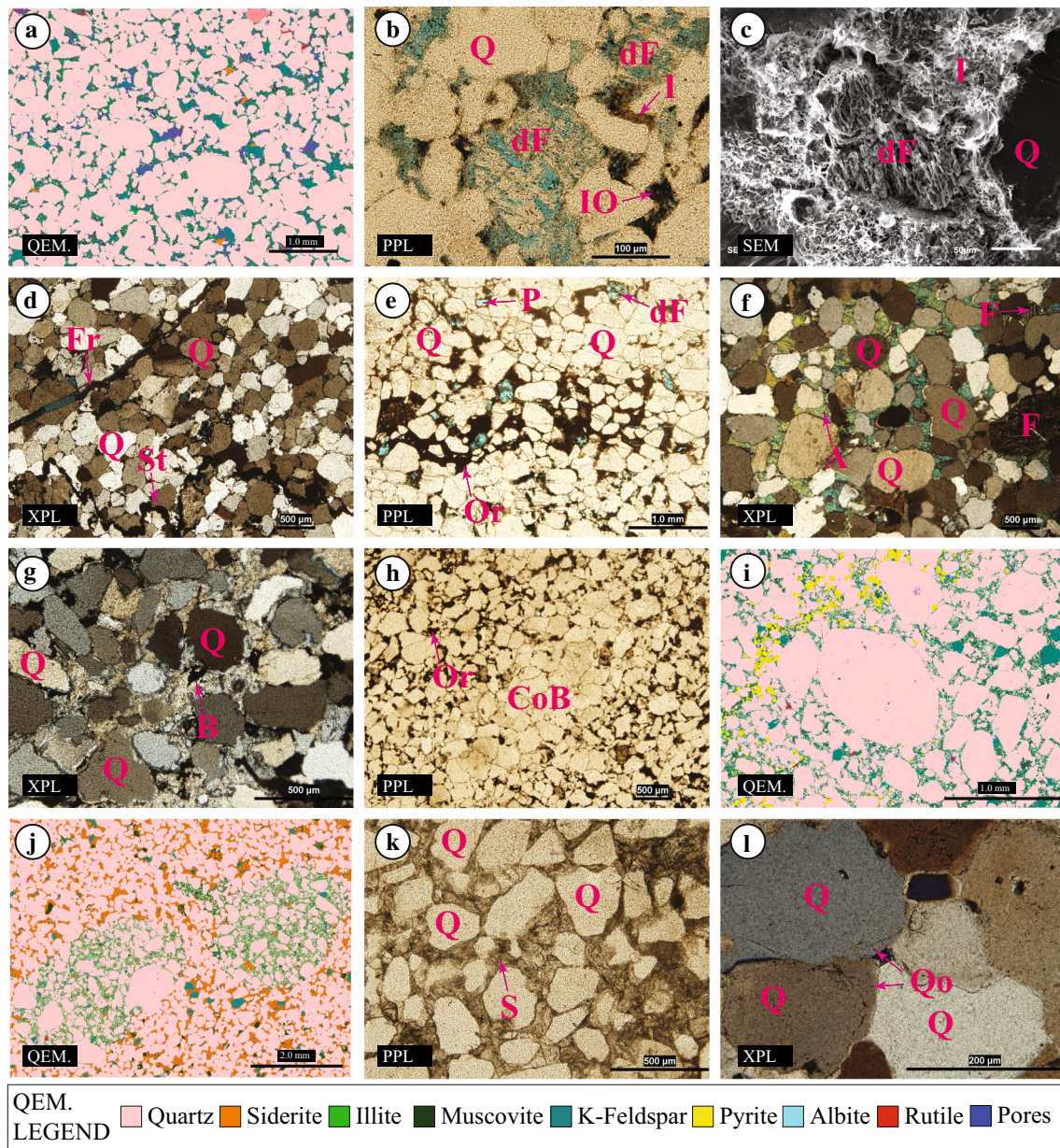


Fig. 8 Representative microdiagenetic processes of all FAs. **a** QEM-SCAN (QEM) image showing pore-filling authigenic illite (green) and trace siderite (orange) cement in the Sm facies of Well A (FA1). **b** Secondary porosity due to feldspar dissolution (dF) associated with pore-filling authigenic illite (I) and iron oxides (IO) under plane-polarized light (PPL). **c** SEM image showing a dissolved feldspar grain (dF) surrounded by authigenic illite (I) in Well A (FA1). **d** Compacted grains associated with a partially filled fracture (Fr) and stylolite (St), and **e** primary (P) and secondary porosity due to feldspar dissolution (dF) affected by pore-filling organic matter (Or) in the Sm facies of Well B (FA2). **f** Complete pore filling by anhydrite (A) and **g** barite

(B) cement in the Sm facies of Well C (FA2). **h** Compaction band (CoB) associated with pore-filling organic matter (Or) in the less compacted part in the Sm facies of Well C (FA2). **i** Pyrite crystals associated with other detrital minerals in the Ds facies of Well B (FA3). **j** QEM-SCAN image of two isolated, matrix-supported partings surrounded by highly siderite-cemented quartz grains in the Ds facies of Well B (FA3). **k** Siderite cement (S) completely filling pore spaces in the Sm facies of Well D (FA4). **l** Optical micrograph under cross-polarized light (XPL) of syntaxial quartz overgrowths (Qo, silica cement) in the Sm facies of Well E (FA4)

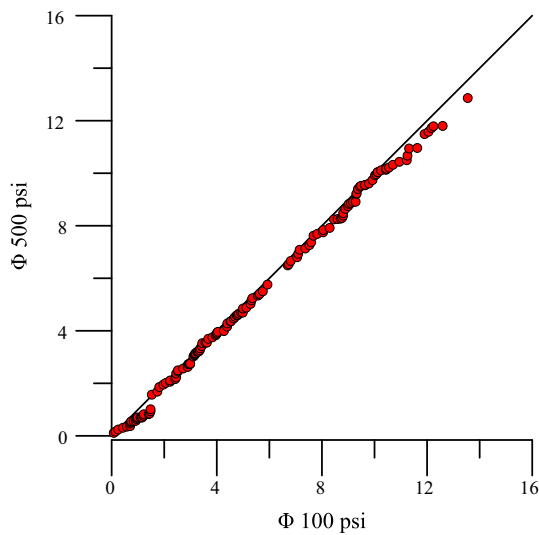


Fig. 9 Q–Q plot of porosity data at 100 psi (helium porosimeter) and at 500 psi (AP-608). Data from both techniques are comparable

organic matter was observed in the matrix in the Dmm facies of Well F.

4.2.4 Porosity and Permeability

Porosity data were acquired using two different techniques—helium porosimeter at 100 psi and an AP-608 at 500 psi. The dual testing was performed to validate the porosity measurements at 500 psi, which were eventually compared with permeability measurements taken under the same confining stress conditions. The porosity results from both techniques were found to be almost comparable (Fig. 9).

4.2.5 Porosity and Permeability Statistics

The statistical summary of the porosity data from each FA (Table 4) shows that fluvial facies (FA1, Well A) had the highest values, reaching up to ~12.86% (average $[m] = \sim 9.37\%$), and the lowest coefficient of variation (CV = 19%). The lowest porosity averages of 0.96% (CV = 52%) and 1.17% (CV = 138%) characterized the subglacial facies of Wells D and F, respectively. The porosity values did not only vary from one FA to another, but they also varied among facies in the same well. For instance, in Well B, the CV ranged from 34% ($m = 2.735\%$) in the Ds and Dcm facies (FA3), and 53% ($m = 6.211\%$) in the Sd facies (FA2), to 67% ($m = 2.508\%$) in the Sd facies (FA2). The porosity data were highly level of variable in the subglacial facies (FA3) of Well F (CV = 138%); however, in general, the porosity data were less heterogeneous than the permeability data.

The averages of the permeability data in the FA ranged from 0.030 mD in the subglacial facies (FA3, Wells B, D and F), the Sd facies (FA2, Well B) and the glaciofluvial facies

Table 4 Statistical summary of the porosity (Φ) and permeability (K) data acquired using AP-608 at 500 psi

Wells	Facies Association	Facies codes	Φ (%)					K (mD)						
			min	max	range	m	SD	CV	min	max	range	m	SD	CV
A	FA1	Sm, Sd, Sr	4.650	12.859	8.209	9.669	1.790	19%	0.047	17.462	17.415	1.926	3.782	196%
B	FA2	Sm	0.470	10.220	9.750	6.211	3.315	53%	0.013	10.783	10.770	2.197	3.969	181%
B	FA2	Sd	0.310	4.880	4.570	2.508	1.685	67%	0.006	0.116	0.110	0.033	0.037	112%
C	FA2	Sm	0.240	10.670	10.430	5.419	3.408	63%	0.002	56.220	56.218	2.075	9.587	462%
B	FA3	Ds, Dcm	1.860	2.060	0.200	2.735	0.921	34%	0.024	0.109	0.085	0.060	0.035	58%
D	FA3	Dmm	0.550	3.960	3.410	0.966	0.507	52%	0.001	0.172	0.171	0.030	0.063	214%
F	FA3	Dmm, Dms, Fm	0.111	5.020	4.909	1.174	1.621	138%	0.007	0.450	0.443	0.155	0.183	119%
E	FA4	Sm, Sd, St, GRfu, GRh	0.760	7.370	6.610	4.407	1.600	36%	0.014	4.214	4.200	0.370	0.737	199%
D*	FA4	Sm	—	—	—	2.735	—	—	—	—	—	0.014	—	—

min: minimum, max: maximum, m: average, SD: standard deviation, CV: coefficient of variation
* only one sample

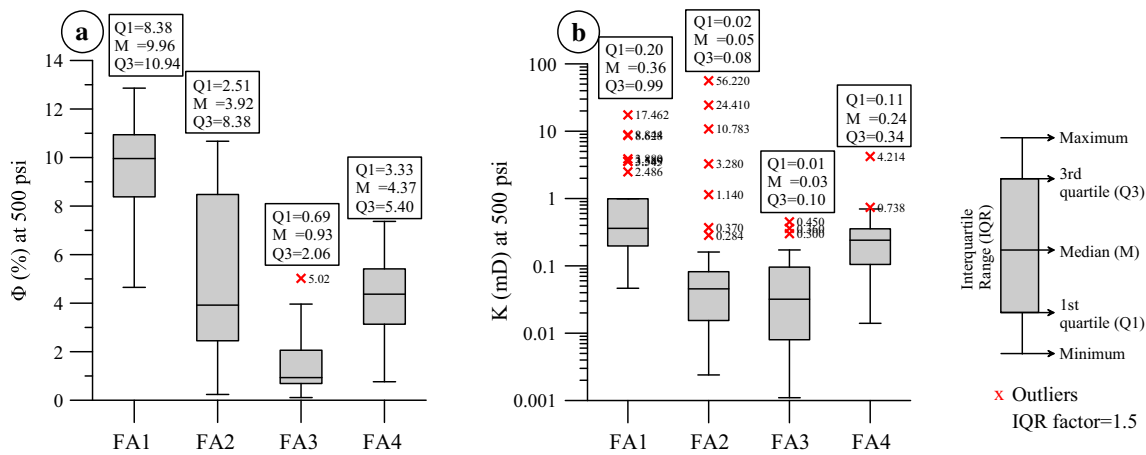
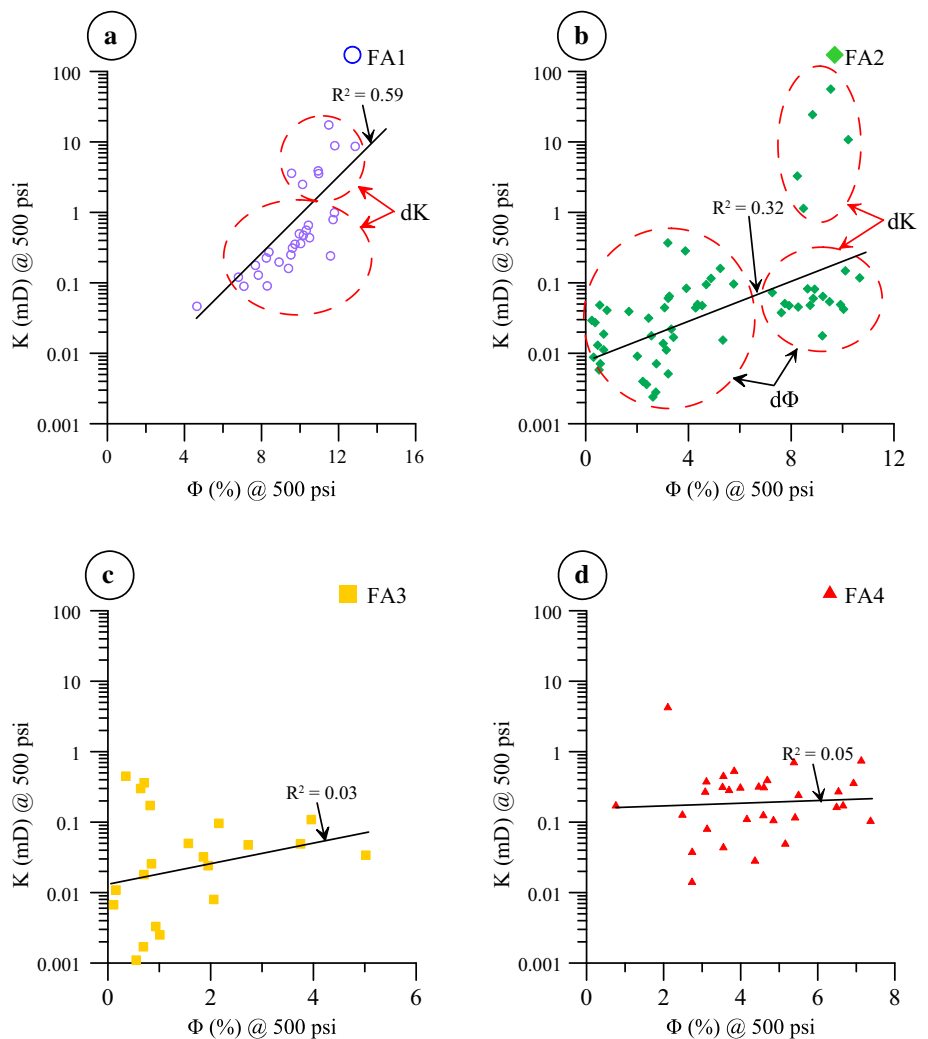


Fig. 10 Box-and-whisker plots of **a** porosity and **b** permeability data at 500 psi of all FAs. FA1: fluvial facies, FA2: glaciolacustrine delta facies, FA3: subglacial facies and FA4: glaciofluvial facies

Fig. 11 Porosity and permeability crossplots of all FAs. FA1: fluvial facies, FA2: glaciolacustrine delta facies, FA3: subglacial facies and FA4: glaciofluvial facies. Dual porosity and permeability ($d\Phi$ and dK , respectively) in FA1 and FA2 associated with primary and secondary porosities and fractures



(FA4, Well E) to 2.197 mD in FA2 of Well B (Table 4). The permeability values of all the FAs were highly variable, with CV values ranging from 58% ($m = 0.060$ mD) in the

glaciolacustrine delta facies (FA2, Well C) to 462% ($m = 2.075$ mD) in the subglacial facies (CV = 214%, Well D). On the other hand, the lowest CV values in the subglacial

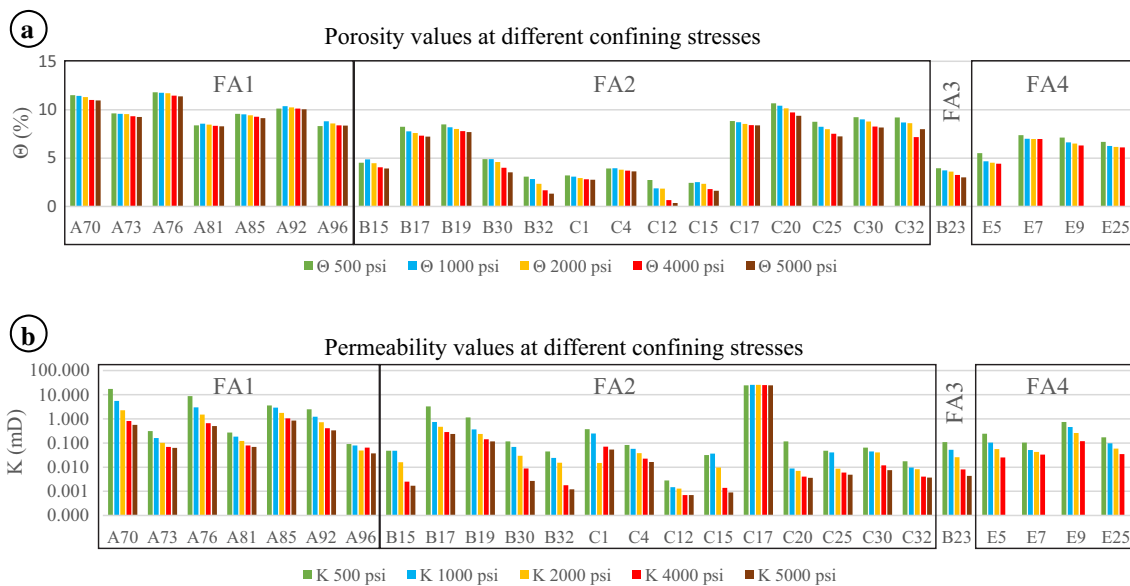


Fig. 12 Porosity and permeability values of selected samples representing four FAs at different confining stresses, ranging from 500 to 5000 psi. The permeability values are much more reduced by increased stress than the porosity values

facies were associated with the Ds and Dcm facies (FA3, Well B). The distributions of the porosity and permeability data, including their first (25%), median (50%) and third (75%) quartiles, are illustrated in Fig. 10a, b; the data outliers for both the porosity and permeability in each FA are indicated. The data shown in Fig. 10 suggest that the highest porosity values were in the fluvial facies (FA1), while the subglacial facies (FA3) was typified by the lowest values. The high heterogeneity observed in the permeability data is indicated by the greater number of outliers compared to the porosity data; however, the permeability values in the fluvial (FA1) and glaciofluvial (FA4) facies were higher than those of the glaciolacustrine delta (FA2) and subglacial (FA3) facies.

4.2.6 Porosity and Permeability Relationships

The relationship between the porosity and permeability data is variable. Crossplots of the porosity (Φ , %, linear scale) and permeability (K, mD, log scale) data show that they are moderately to weakly correlated in the fluvial (FA1, $R^2 = 0.59$; Fig. 11a) and in the glaciolacustrine (FA2, $R^2 = 0.32$; Fig. 11b) facies, where dual porosity/permeability occurs. The porosity and permeability correlations in the glaciofluvial outwash (FA4, $R^2 = 0.05$; Fig. 11d) and subglacial (FA3, $R^2 = 0.03$; Fig. 11c) facies are negligible.

4.2.7 Confining Stress Effects on Porosity and Permeability

The porosity values acquired under various confining stresses showed a slight decrease in each sample of the fluvial (FA1,

Well A) and glaciofluvial (FA4, Well E) facies. When the stress increased, the porosity values decreased, from 1 to 5% of the original values in FA1, and from 5 to 19% in FA4 (Fig. 12a). The permeability of these facies also decreased, but with a much higher ratio than seen in the porosity. For instance, the permeability value in one of the FA1 samples decreased, from 17.46 mD at 500 psi to 0.56 mD at 5000 psi (Fig. 12b, Sample A70) and from 0.24 mD at 500 psi to 0.025 mD at 4000 psi in one of the FA4 samples (Fig. 12b, Sample E5).

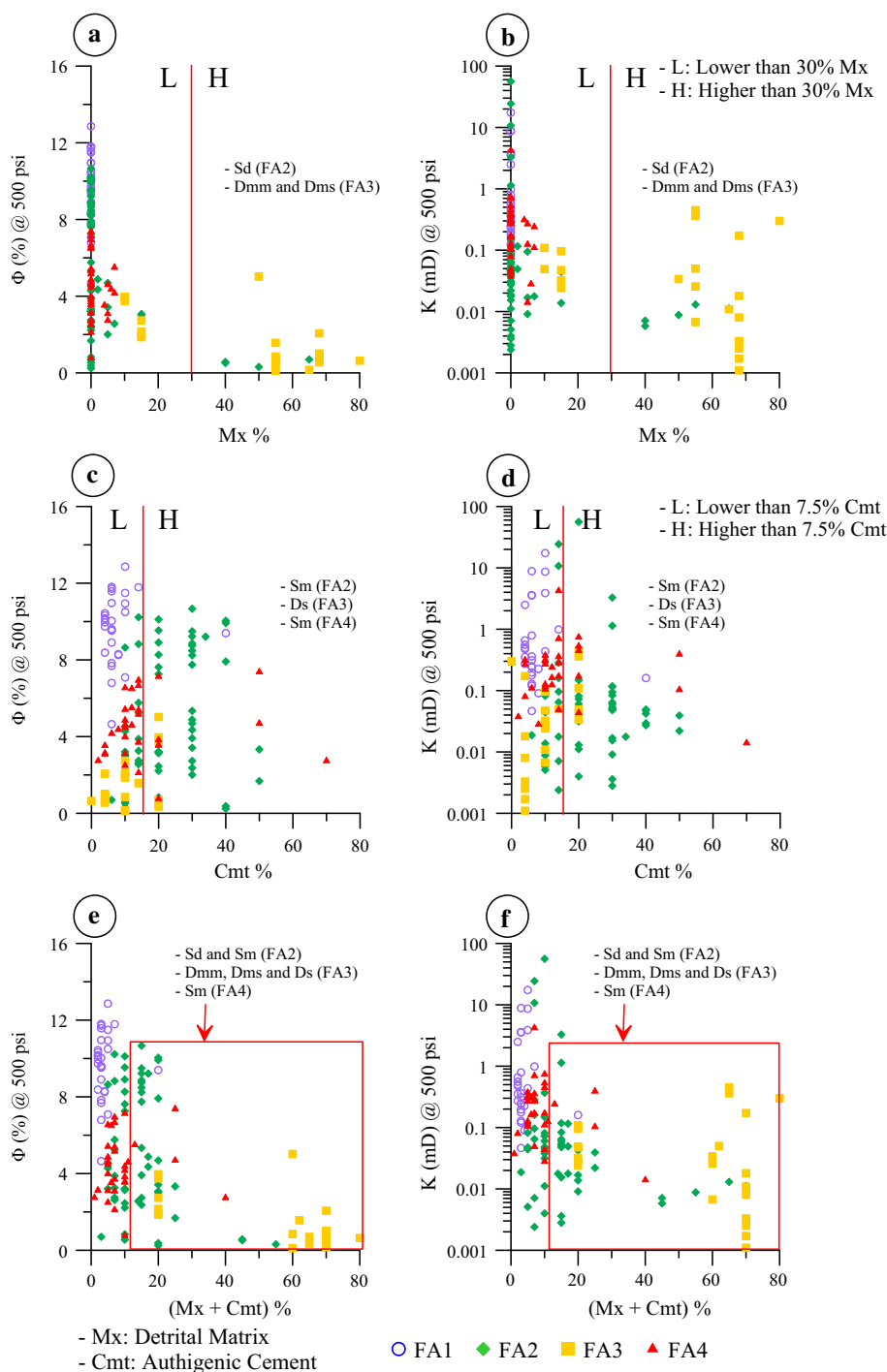
The porosity values in the glaciolacustrine delta facies (FA2) showed different behavior toward the stresses. They decreased to less than 40% of the original values when the stress increased from 500 psi to 5000 psi in some of FA2 samples (Fig. 12a, Samples B32 and C12). Apart from one sample (C17, FA2) with a permeability value of >24 mD, the permeability was significantly reduced when the stress was increased from 500 psi to 5000 psi. The reduction ratios ranged from 75 to 98% of the original values in both FA2 and FA3.

5 Interpretation and Discussion

5.1 Depositional Facies and Reservoir Quality

The Upper Ordovician Sarah Formation in the present study is characterized by a variety of depositional facies, the distribution of which might be related to the basement morphology beneath the formation. The glaciolacustrine delta (FA2) and subglacial (FA3) facies were located above base-

Fig. 13 Relationships between **a, b** detrital matrix, **c, d** cement, **e, f** the total of both agents and porosity and permeability for all FAs. The porosity and permeability in the fluvial (FA1), glaciofluvial (FA4) and Sm facies of the glaciolacustrine delta (FA2) facies show no/slight influences of the matrix and cement

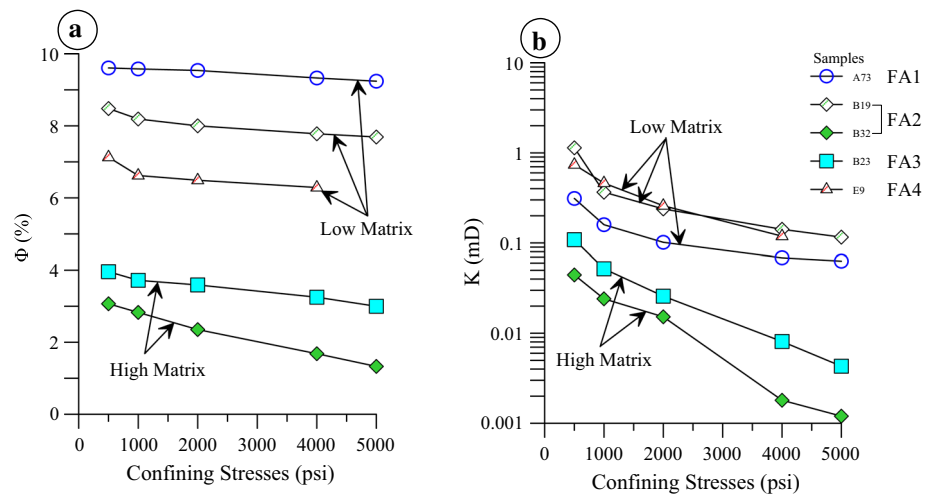


ment depressions, while the fluvial (FA1) and glaciofluvial outwash (FA4) facies were located above basement highs. This variety of depositional settings explains the heterogeneity of the reservoir rocks in the formation. The detrital mineralogy of the framework grains and matrix, the texture (grain size, sorting, etc.) and primary porosity inherited from these depositional settings have exerted significant control

on the reservoir quality and have also influenced the post-depositional controls [34, 35].

The matrix content (clay and silt), predominantly illite (Fig. 7i), is the depositional factor that has most affected the reservoir quality (Fig. 13a, b) in the Dmm and Dms (FA3, Fig. 7h–j) and in Sd (FA2, Fig. 7c) facies, with the permeability values being mostly equal to, or less than, 0.1 mD. Figure 11b indicates a strong correlation between porosity

Fig. 14 Effects of increasing confining stress on **a** porosity and **b** permeability values. Matrix content increases in the subglacial facies (FA3) and the Sd facies of the glaciolacustrine delta facies (FA2), thus the porosity/permeability losses were likely due to compressibility



and permeability in the Sd facies (FA2). The relationship between these properties in matrix-rich intervals depends on the lithology and/or diagenesis, but it is not a function of porosity [36].

Grain size and sorting are the other depositional controls affecting reservoir quality [e.g., 37]. The highest porosity and permeability values (Fig. 10a, b) were associated with the fine- to medium-grained sandstones (Fig. 4a, b) of the fluvial facies (FA1). On the contrary, the lowest permeability values (Fig. 10b) were associated with the Ds, Dcm, Dmm and Dms facies (FA3), characterized by hybrid grain-sized and poorly sorted sandstones, which are also characteristics of the glaciofluvial (FA4; Fig. 4) and some of the glaciolacustrine delta (FA2; Fig. 4) facies.

Grain-size distribution and sorting are initially determined by the sediment transport mechanism [34]. Prior to diagenesis, preservation of the primary porosity is a function of grain size, sorting and packing. In this study, the subarkosic fluvial (FA1; Fig. 7a) and quartz arenitic Sm facies (Fig. 7d) of the glaciolacustrine delta (FA2) facies, which contained little to no matrix, was preserved in localized intervals. These facies have also suffered grain compaction caused by overburden stress, although the primary porosity, which exists with the presence of microfractures (Fig. 8d), was preserved (Fig. 8e).

5.2 Diagenesis and Reservoir Quality

The diagenetic processes observed in the studied core samples of the Upper Ordovician Sarah Formation in the Rub' al Khali Basin indicate that the formation has experienced burial diagenesis, including grain compaction (mechanical and chemical), dissolution (of feldspars) and cementation (authigenic illite, anhydrite, calcite, barite, siderite, and silica overgrowth). These processes are primarily influenced by the depositional setting [35, 38].

Grain mineralogy and texture (i.e., grain size, distribution, shape and sorting) play significant roles in sediment compressibility and have substantial effects on the development of porosity and permeability through burial depth [39]. A one-dimensional compression experiment conducted on conventional sand has shown that the highest porosity loss occurs in fine-grained, clay-rich sands [40]. Our experiments on this unconventional tight sandstone also showed that the higher the matrix content, the higher the loss of porosity and permeability due to the increase in confining stress. Therefore, a significant decrease in porosity and permeability can be attributed to the matrix-rich samples of the subglacial facies (Fig. 14, Sample B23) and the Sd facies of the glaciolacustrine delta (Fig. 14, Sample B32).

The compaction and cementation processes considered to be porosity-/permeability-reducing factors varied significantly among the studied facies. A general understanding of the reservoir-quality controlling factors would enhance reservoir evaluation. Despite the variable depositional settings, these factors are naturally heterogeneous, even in a single depositional setting. After deposition, the sediment grains are packed, becoming mechanically compacted with subsequent overlying deposition. Suture contacts and stylolites (Fig. 8d), formed by chemical compaction and pressure solution, could be developed with the absence of cement and matrix components. Grain compaction appears to have negatively influenced the reservoir quality more than the cement or matrix (Fig. 13e, f) in the fluvial (FA1), most of the glaciofluvial (FA4) and the Sm facies of the glaciolacustrine delta (FA2) facies in this study.

Anhydrite (Fig. 8f) and barite (Fig. 8g) cements in these studied FAs are limited to the Sm facies of the glaciolacustrine delta (FA2) facies, while siderite cement occurred in significant amounts in the glaciofluvial (FA4, Well D) and subglacial (Ds, Well B; Table 3) facies. These types of cement occluded the pores and pore throats and, subse-

quently, reduced the porosity and permeability in the facies. Authigenic illite presents as a pore-filling and grain-coating clay mineral in the fluvial facies (FA1; Fig. 8a, c). Secondary porosity development was also likely enhanced by feldspar grain dissolution in FA1 and 4. However, the dissolution of K-feldspar not only produced additional pores, but also released potassium, which is a major source for the illitization processes [35, 41]. Grain-coating illite might have prevented quartz overgrowth, thereby allowing the preservation of intergranular porosity [e.g., 41]. Illitization can also occlude pore throats and, consequently, reduce permeability. The occurrence of quartz overgrowth (Fig. 81) likely reduced both the porosity and the permeability in the glaciofluvial facies (FA4), where only trace amounts of authigenic illite are present.

This study was not intended to quantify diagenetic processes and products, but rather to discuss the importance of their roles in preserving or diminishing the reservoir quality of the Sarah Formation in the Rub' al Khali Basin. Both depositional and diagenetic controls on porosity and permeability have acted, individually or together, on the studied facies, and each control has had either a direct influence on the porosity and/or permeability, or an indirect influence by affecting other diagenetic processes. The natural heterogeneity of the controls on reservoir quality, and the scale of their investigation, are still major issues; however, quantifying both depositional and diagenetic controls, and defining the relationship between them among several formations in one location, or one formation in various locations, within predefined facies and FAs, is recommended for addressing reservoir quality, evaluation and prediction.

6 Conclusions

Four FAs, including fluvial (FA1), glaciolacustrine delta (FA2), subglacial (FA3) and glaciofluvial (FA4), were investigated in order to evaluate the depositional and diagenetic controls involved in the reservoir quality of the Sarah Formation in the Rub' al Khali Basin. FA1, a subarkose, has the best reservoir quality, but this quality was partially negatively controlled by grain compaction, and pore filling and grain coating by authigenic illite. The porosity of FA1 was likely enhanced by fractures and feldspar dissolution, leading to the development of dual porosity/permeability. Dual porosity was present in the quartz to sublithic arenites of FA2 as primary and secondary porosity; however, the reservoir quality of FA2 was limited by their association with grain compaction, anhydrite and barite cement in the Sm facies, as well as matrix content (detrital illite) and compressibility in the Sd facies. The poorest reservoir quality, characterized by FA3, might have been caused by poor grain sorting, a high matrix component and compressibility in the Dmm and

Dms facies. Siderite cementation in the Dcm and Ds facies also likely reduced the porosity. FA4 was a sublithic arenite, and its reservoir quality was negatively influenced by poor grain sorting, grain compaction, quartz overgrowth, authigenic illite and siderite cementation.

It is strongly recommended that the analysis of facies and FAs, and the quantification of diagenetic factors, be integrated to provide a better understanding of the most influential factors controlling reservoir quality. This might eventually help guide the exploration and development of tight sandstone reservoirs in the subsurface Sarah Formation and its age-equivalents elsewhere.

Acknowledgements We sincerely acknowledge the support provided by the King Fahd University of Petroleum and Minerals (KFUPM). This work was supported by the King Abdulaziz City for Science and Technology as part of the National Science, Technology, and Innovation Plan (NSTIP Project # 14-OIL468-04) through the Science and Technology Unit at KFUPM. The samples used in this study were provided by the Ministry of Energy, Industry and Mineral Resources, Saudi Arabia. The SEM and XRD analyses were conducted at the Center for Engineering Research (CER), Research Institute, KFUPM. The support of these organizations at every stage of the work is fully acknowledged. The authors also thank Mr. Hatem Mohammed and Mr. Abdul-Rasheed Isiaka, from CER, for their assistance in the SEM and XRD analyses.

References

1. Holditch, S.A.: Tight gas sands. *J. Pet. Technol.* **58**, 86–93 (2006)
2. Jiang, Z.X.; Li, Z.; Li, F.; Pang, X.Q.; Yang, W.; Liu, L.F.; Jiang, F.J.: Tight sandstone gas accumulation mechanism and development models. *Pet. Sci.* **12**, 587–605 (2015). <https://doi.org/10.1007/s12182-015-0061-6>
3. Hayton, S.; Heine, C.; Gratto, B.E.: Tight gas exploration in Saudi Arabia. In: SPE Deep Gas Conference and Exhibition. Society of Petroleum Engineers (2010)
4. Lai, J.; Wang, G.; Wang, Z.; Chen, J.; Pang, X.; Wang, S.; Zhou, Z.; He, Z.; Qin, Z.; Fan, X.: A review on pore structure characterization in tight sandstones. *Earth Sci.* **177**, 436–457 (2018). <https://doi.org/10.1016/j.earscirev.2017.12.003>
5. Sahin, A.: Unconventional natural gas potential in Saudi Arabia. In: SPE Middle East Oil and Gas Show and Conference. Society of Petroleum Engineers (2013)
6. Al-Mahmoud, M.J.; Al-Ghamdi, I.: An overview of tight gas reservoirs in Saudi Arabia. In: Second EAGE Middle East Tight Gas Reservoirs Workshop. EAGE (2010)
7. British Petroleum: BP statistical review of world energy 2017 (2017)
8. Gier, S.; Worden, R.H.; Johns, W.D.; Kurzweil, H.: Diagenesis and reservoir quality of Miocene sandstones in the Vienna Basin, Austria. *Mar. Pet. Geol.* **25**, 681–695 (2008). <https://doi.org/10.1016/j.marpetgeo.2008.06.001>
9. Zhang, Y.; Pe-Piper, G.; Piper, D.J.W.: How sandstone porosity and permeability vary with diagenetic minerals in the Scotian Basin, offshore eastern Canada: implications for reservoir quality. *Mar. Pet. Geol.* **63**, 28–45 (2015). <https://doi.org/10.1016/j.marpetgeo.2015.02.007>
10. Alqubalee, A.; Abdullatif, O.; Babalola, L.; Makkawi, M.: Characteristics of Paleozoic tight gas sandstone reservoir: integration of lithofacies, paleoenvironments, and spectral gamma-ray analyses,



- Rub' al Khali Basin, Saudi Arabia. *Arab. J. Geosci.* (2019). <https://doi.org/10.1007/s12517-019-4467-0>
11. Konert, G.; Afifi, A.M.; Al-Hajri, S.A.; Droste, H.J.: Paleozoic stratigraphy and hydrocarbon habitat of the Arabian plate. *GeoArabia* **6**, 407–442 (2001). <https://doi.org/10.1306/M74775C24>
 12. Stoesser, D.B.; Camp, V.E.: Pan-African microplate accretion of the Arabian Shield. *Bull. Geol. Soc. Am.* **96**, 817–826 (1985). <https://doi.org/10.1130/0016-7606>
 13. Stewart, S.A.: Structural geology of the Rub' Al-Khali Basin, Saudi Arabia. *Tectonics* **35**, 2417–2438 (2016). <https://doi.org/10.1002/2016TC004212>
 14. Stern, R.J.; Johnson, P.: Continental lithosphere of the Arabian Plate: a geologic, petrologic, and geophysical synthesis. *Earth-Sci. Rev.* **101**, 29–67 (2010). <https://doi.org/10.1016/j.earscirev.2010.01.002>
 15. Dyer, R.A.; Hussein, M.: The western Rub'Al-Khali Infracambrian Graben System. In: Middle East Oil Show. Society of Petroleum Engineers, Bahrain (1991)
 16. Vaslet, D.: Upper ordovician glacial deposits in Saudi-Arabia. *Episodes* **13**, 147–161 (1990)
 17. McClure, H.A.: Early paleozoic glaciation in Arabia. *Palaeogeogr. Palaeoclimatol. Palaeoecol.* **25**, 315–326 (1978)
 18. Vaslet, D.; Kellogg, K.S.; Berthiaux, A.; Le Strat, P.; Vincent, P.L.: Explanatory notes to the geologic map of the Baq'a Quadrangle, Kingdom of Saudi Arabia. *Geosci. Map GM-116 C*, Scale 1250,000. 1–45 (1987)
 19. Williams, P.L.; Vaslet, D.; Johnson, P.R.; Berthiaux, A.; Le Strat, P.; Fomiguet, J.: Geologic map of the Jabal Habashi quadrangle, sheet 26F. Kingdom Saudi Arab. Saudi Arab. Deputy Minist. Miner. Resour. *Geosci. Map-GM-98 A*, Scale 1250,000 (1986)
 20. Clark-Lowes, D.D.: Sedimentology and mineralization potential of Saq and Tabuk formations. *Imp. Coll. Sci. Technol. London, Open-File Rep. CRC/IC. 7* (1980)
 21. SSC.: Phanerozoic Stratigraphy of Saudi Arabia Part 1. In: Saudi Geological Survey. Special Publications, 1st edn, pp 1–69 (2013)
 22. Abu-Ali, M.; Littke, R.: Paleozoic petroleum systems of Saudi Arabia: a basin modeling approach. *GeoArabia* **10**, 131–168 (2005)
 23. Senalp, M.; Al-Laboun, A.: New evidence on the Late Ordovician glaciation in central Saudi Arabia. *Saudi Aramco J. Technol. Spring.* **14**, 11–40 (2000)
 24. Tofaif, S.; Le Heron, D.P.; Melvin, J.: Development of a palaeovalley complex on a Late Ordovician glaciated margin in NW Saudi Arabia. *Geol. Soc. London Spec. Publ.* **475**, 81–107 (2018). <https://doi.org/10.1144/sp475.8>
 25. Clark-Lowes, D.D.: Arabian glacial deposits: recognition of palaeovalleys within the Upper Ordovician Sarah Formation, Al Qasim district, Saudi Arabia. *Proc. Geol. Assoc.* **116**, 331–347 (2005). [https://doi.org/10.1016/S0016-7878\(05\)80051-3](https://doi.org/10.1016/S0016-7878(05)80051-3)
 26. El-Deek, I.; Abdullatif, O.; Korvin, G.: Heterogeneity analysis of reservoir porosity and permeability in the Late Ordovician glaciofluvial Sarah Formation paleovalleys, central Saudi Arabia. *Arab. J. Geosci.* **10**, 400 (2017). <https://doi.org/10.1007/s12517-017-3146-2>
 27. Babiker, J.M.A.; Hariri, M.M.; Abdullatif, O.; Korvin, G.: Types and nature of fracture associated with Late Ordovician paleochannels of glaciofluvial Sarah Formation, Qasim region. Central Saudi Arabia. *Arab. J. Geosci.* **10**, 146 (2017). <https://doi.org/10.1007/s12517-017-2922-3>
 28. Craigie, N.W.; Rees, A.; MacPherson, K.; Berman, S.: Chemostratigraphy of the Ordovician Sarah Formation, North West Saudi Arabia: an integrated approach to reservoir correlation. *Mar. Pet. Geol.* **77**, 1056–1080 (2016). <https://doi.org/10.1016/j.marpetgeo.2016.07.009>
 29. Bassis, A.; Hinderer, M.; Meinhold, G.: Petrography and geochemistry of Palaeozoic quartz-rich sandstones from Saudi Arabia: implications for provenance and chemostratigraphy. *Arab. J. Geosci.* **9**, 400 (2016). <https://doi.org/10.1007/s12517-016-2412-z>
 30. Al-Harbi, O.A.; Khan, M.M.: Source and origin of glacial paleovalley-fill sediments (Upper Ordovician) of Sarah Formation in central Saudi Arabia. *Arab. J. Geosci.* **4**, 825–835 (2011)
 31. Bassis, A.; Hinderer, M.; Meinhold, G.: New insights into the provenance of Saudi Arabian Palaeozoic sandstones from heavy mineral analysis and single-grain geochemistry. *Sediment. Geol.* **333**, 100–114 (2016). <https://doi.org/10.1016/j.sedgeo.2015.12.009>
 32. Moscardiello, A.; Spaak, P.; Jourdan, A.; Azzouni, A.-H.: The ordovician glaciation in Saudi Arabia—exploration challenges part 1. *Geology (Outcrop, Subsurface, Analogues)*. In: AAPG International Conference and Exhibition., Search and Discovery Article #50175 (2008)
 33. Briner, A.P.A.P.; Hulver, M.; Azzouni, A.; Harvey, C.: Regional reservoir quality of a tight gas play: the ordovician Sarah Formation in the Rub'Al Khali Basin of Southern Saudi Arabia. In: Second EAGE Middle East (2010)
 34. Haile, B.G.; Klausen, T.G.; Czarniecka, U.; Xi, K.; Jahren, J.; Hellevang, H.: How are diagenesis and reservoir quality linked to depositional facies? A deltaic succession, Edgeøya, Svalbard. *Mar. Pet. Geol.* **92**, 519–546 (2018). <https://doi.org/10.1016/j.marpetgeo.2017.11.019>
 35. Bjørlykke, K.: Relationships Between Depositional Environments, Burial History and Rock Properties: Some Principal Aspects of Diagenetic Process in Sedimentary Basins. Elsevier, Amsterdam (2014)
 36. Dewhurst, D.N.; Aplin, A.C.; Sarda, J.-P.; Yang, Y.: Compaction-driven evolution of porosity and permeability in natural mudstones: an experimental study. *J. Geophys. Res. Solid Earth.* **103**, 651–661 (1998). <https://doi.org/10.1029/97JB02540>
 37. English, K.L.; English, J.M.; Bonnell, L.M.; Lander, R.H.; Hollis, C.; Redfern, J.; Guiridham, C.; Garnham, J.; Yahia Cherif, R.: Controls on reservoir quality in exhumed basins—an example from the Ordovician sandstone, Illizi Basin, Algeria. *Mar. Pet. Geol.* **80**, 203–227 (2017). <https://doi.org/10.1016/j.marpetgeo.2016.11.011>
 38. Morad, S.; Ketzer, J.M.; DeRos, F.: Spatial and temporal distribution of diagenetic alterations in siliciclastic rocks: implication for mass transfer in sedimentary basins. *Sedimentology* **47**, 95–120 (2000). <https://doi.org/10.1046/j.1365-3091.2000.00007.x>
 39. Mahmic, O.; Dypvik, H.; Hammer, E.: Diagenetic influence on reservoir quality evolution, examples from Triassic conglomerates/arenites in the Edvard Grieg field, Norwegian North Sea. *Mar. Pet. Geol.* **93**, 247–271 (2018). <https://doi.org/10.1016/j.marpetgeo.2018.03.006>
 40. Chuhan, F.A.; Kjeldstad, A.; Bjørlykke, K.; Høeg, K.: Experimental compression of loose sands: relevance to porosity reduction during burial in sedimentary basins. *Can. Geotech. J.* **40**, 995–1011 (2003). <https://doi.org/10.1139/t03-050>
 41. Al-Ramadan, K.: Illitization of Smectite in Sandstones: the Permian Unayzah Reservoir, Saudi Arabia. *Arab. J. Sci. Eng.* **39**, 407–412 (2014). <https://doi.org/10.1007/s13369-013-0913-6>
 42. Al-Husseini, M.: Update to late triassic-jurassic stratigraphy of Saudi Arabia for the middle east geologic time scale. *GeoArabia* **14**, 145–186 (2009)
 43. Ruban, D.A.; Al-Husseini, M.I.; Iwasaki, Y.: Review of middle east Paleozoic plate tectonics. *GeoArabia.* **12**, 35–56 (2007)
 44. Ziegler, M.: Late Permian to Holocene Paleofacies Evolution of the Arabian Plate and its Hydrocarbon Occurrences. *GeoArabia* **6**, 445–504 (2001)

